First-principles study of the tunnel magnetoresistance effect with Cr-doped RuO$_2$ electrode

Katsuhiro Tanaka[1], Takuya Nomoto[2,3] and Ryotaro Arita[3,4]

[1]*Department of Physics, University of Tokyo, Hongo, Bunkyo-ku, Tokyo 113-0033, Japan*
[2]*Department of Physics, Tokyo Metropolitan University, Hachioji, Tokyo 192-0397, Japan*
[3]*Research Center for Advanced Science and Technology, University of Tokyo, Komaba, Meguro-ku, Tokyo 153-8904, Japan*
[4]*Center for Emergent Matter Science, RIKEN, Wako, Saitama 351-0198, Japan*

We investigate the functionality of the Cr-doped RuO$_2$ as an electrode of the magnetic tunnel junction (MTJ), motivated by a recent experiment showing that Cr doping into rutile-type RuO$_2$ is an effective tool to easily control its antiferromagnetic order and the resultant magnetotransport phenomena. We perform first-principles calculation of the tunnel magnetoresistance (TMR) effect in the MTJ based on the Cr-doped RuO$_2$ electrodes. We find that a finite TMR effect appears in the MTJ originating from the momentum-dependent spin splitting in the electrodes, which suggests that RuO$_2$ with Cr doping will function effectively as the electrode of the MTJ. We also show that this TMR effect can be qualitatively captured by the local density of states inside the tunnel barrier.

I. INTRODUCTION

The tunnel magnetoresistance (TMR) effect is a spin-dependent transport phenomenon observed in a magnetic tunnel junction (MTJ), a multilayered system consisting of insulating thin films sandwiched by magnetic electrodes [1]. The tunnel resistance can differ when the magnetic moments of two magnetic electrodes align parallelly or antiparallelly.

The TMR effect has long been discussed with ferromagnetic electrodes [1–23] since it has been believed that macroscopic spin polarization is essential to generate a TMR effect. However, recent studies have revealed that MTJs with antiferromagnets can also exhibit a finite TMR effect [24–42]. Particularly, the antiferromagnets breaking the time-reversal symmetry macroscopically are promising materials to show the TMR effect; when the magnetic order of an antiferromagnet breaks the time-reversal symmetry macroscopically, namely, when a magnetically ordered state does not return to the original state after the time-reversal operation and succeeding translation or inversion operations, a finite spin splitting in the momentum space is generated [43–48]. When such an antiferromagnet is used for the electrode of the MTJ, the momentum-dependent spin splitting contributes to generating the difference in the transmission of two configurations. The MTJs using such antiferromagnets have been discussed theoretically [24,29–32,34,35,37–40], and a finite TMR effect has been actually observed in experiments [24,32,40].

A typical candidate material whose antiferromagnetic structure breaks the time-reversal symmetry macroscopically is the rutile-type RuO$_2$. Recently, it has been experimentally proposed that RuO$_2$ possess the collinear antiferromagnetic structure [49,50]. Triggered by this proposal, its spin splitting nature in the momentum space [44,51] and the magnetotransport phenomena such as the anomalous Hall effect [46,52] or the Néel spin current [53] have been discussed. As for the TMR effect, the TMR ratio has been theoretically calculated in the RuO$_2$(001)/TiO$_2$/RuO$_2$- [29], RuO$_2$(110)/TiO$_2$/RuO$_2$- [37], and RuO$_2$/TiO$_2$/CrO$_2$-MTJs [38,39], as well as in the argument based on the properties of the electrode [30].

However, several studies argue that the magnetism in RuO$_2$ is very weak [54] and even nonmagnetic experimentally [55,56], which might prevent us from applying RuO$_2$ to the TMR effect or other spintronic phenomena. Here, we avoid the potentailly weak antiferromagnetism of RuO$_2$ while preserving the time-reversal symmetry-breaking magnetic structure in rutile systems by element substitution. A recent experiment investigated the physical properties of Cr-doped RuO$_2$ [57] demonstrating that the Cr-doped RuO$_2$ exhibits a distinct anomalous Hall effect even in a small or zero magnetic field. This experiment has suggested that doping Cr is a possible way to easily manipulate the magnetic order and magnetotransport properties of RuO$_2$ systems.

In this paper, we discuss the functionalities of the Cr-doped RuO$_2$ as an electrode of the MTJ. First we perform first-principles calculation of the Cr-doped RuO$_2$ and show that Cr-doped RuO$_2$ has the spin splitting depending on the momentum. Then, we perform first-principles calculation of the TMR effect with Ru$_{1-x}$Cr$_x$O$_2$/TiO$_2$/Ru$_{1-x}$Cr$_x$O$_2$ MTJ and find that the Cr-doped RuO$_2$ shows a finite TMR effect owing to the spin-splitting structure.

This paper will also have a practical significance in designing MTJs with compensated magnets. There have been proposals that the TMR properties can be evaluated by focusing on the local density of states (LDOS) in the MTJs [10,12,13,18,26]. For example, an early study evaluated the transmission by the LDOS at the interface of the MTJs and the decaying factor [10]. To further advance the utility of the LDOS, we have recently proposed a real-space method to evaluate the TMR effect qualitatively with the LDOS inside the tunnel barrier in model calculations [33]. By using this method, the calculation of the transmission, which usually
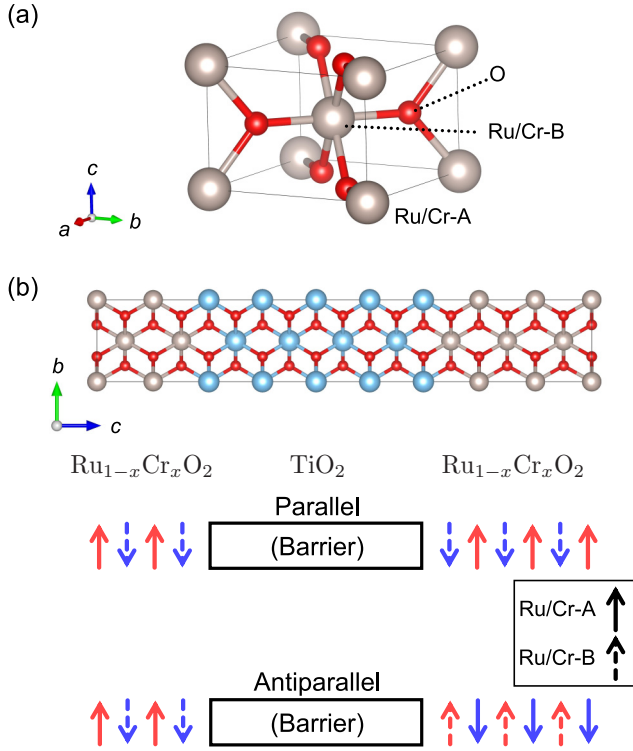
FIG. 1. (a) Crystal structure of $Ru_{1-x}Cr_xO_2$. (b) Crystal structure of the $Ru_{1-x}Cr_xO_2/TiO_2/Ru_{1-x}Cr_xO_2$ magnetic tunnel junction and schematics of the alignments of the magnetic moments for the parallel and antiparallel configurations. Arrows and arrows with broken lines represent the magnetic moments of the Ru/Cr-A and Ru/Cr-B sites, respectively.

demands high computational cost in first-principles calculations, could be skipped. However, that proposal is based on the idealized lattice model and it is not trivial to apply this estimation, in terms of the local density of states, to more realistic MTJ systems, particularly the TMR effect with compensated magnets. We verify the applicability of the estimation method based on the LDOS.

II. SYSTEM AND METHOD

A. Density functional theory calculations of Cr-doped RuO₂ and tunnel magnetoresistance effect with Cr-doped RuO₂

We use the rutile-type RuO_2 whose Ru sites are partially substituted for Cr, $Ru_{1-x}Cr_xO_2$, as the electrode of the MTJ. RuO_2 has the tetragonal crystal structure (space group: $P4_2/mnm$) with two inequivalent Ru sites, Ru-A and Ru-B, in a unit cell [Fig. 1(a)]. We use the a- and c-axis lattice constants of RuO_2 as $a_{RuO_2} = 4.4919$ Å and $c_{RuO_2} = 3.1066$ Å, respectively. The position of oxygen atom is $x = 0.3058$ for RuO_2. The crystal structure and the lattice parameters of RuO_2 are obtained from the Inorganic Crystal Structure Database (ICSD) (Collection Code 15071) [58].

As a barrier layer of the MTJ, we use the rutile-type TiO_2. Specifically, we calculate the TMR effect in the $Ru_{1-x}Cr_xO_2/TiO_2/Ru_{1-x}Cr_xO_2$ MTJ. Here, $Ru_{1-x}Cr_xO_2$ and TiO_2 are stacked along (001) direction [Fig. 1(b)]. For TiO_2, the in-plane lattice constant is matched to a_{RuO_2}, and c-axis

length is $c_{TiO_2} = 2.9589$ Å. The interface between RuO_2 and TiO_2 is given by the average of c_{RuO_2} and c_{TiO_2}. The position of oxygen atom for TiO_2 is $x = 0.3057$. The crystal structure and the lattice parameters of TiO_2 are obtained from the ICSD (Collection Code 9161) [58].

The TMR effect is calculated based on the scattering theory approach [59] with the Landauer–Büttiker formula [60–63]. First, we separate the whole MTJ into three parts: the left and right leads, and the scattering region. Here, the left and right leads are $Ru_{1-x}Cr_xO_2$, and the scattering region is nine monolayers (MLs) of TiO_2 with four MLs and five MLs of $Ru_{1-x}Cr_xO_2$ on its left and right sides, respectively. We calculate the electronic structure of each of these three parts. Then, we construct the MTJ attaching these three parts and calculate the transmission.

To obtain the electronic structure, we perform the density functional theory (DFT) calculations [64,65] using the QUANTUM ESPRESSO (QE) package [66,67]. We use the norm-conserved pseudopotential obtained from PSEUDODOJO [68,69]. The exchange correlation is taken in by the Perdew-Berke-Ernzerhof type generalized gradient approximation [70]. The energy cutoff for the wave-function is 110 Ry, and that for the charge density is 440 Ry. We take $15 \times 15 \times 20$ and $15 \times 15 \times 1$ $\mathbf{k}$ points for the self-consistent field (scf) calculation of the lead and the scattering region, respectively. We do not consider the effect of spin-orbit coupling or the additional Coulomb interaction $+U$. We use the virtual crystal approximation (VCA) [71,72] to substitute Ru with Cr [73]. We mix the potential of Ru and Cr, V_{Ru} and V_{Cr}, respectively, to generate the potential of the virtual atom $Ru_{1-x}Cr_x$, $V_{Ru_{1-x}Cr_x}(x)$. The mixed potential is written as $V_{Ru_{1-x}Cr_x}(x) = (1-x)V_{Ru} + xV_{Cr}$. For the antiparallel configuration, we attach the copy of the scattering region with its magnetic structure inverted and calculate the electronic structure of the doubled scattering region to deal with the electronic and magnetic structures at the boundary between the leads and the scattering region properly. When we calculate the transmission, the doubled supercell is cut in half and restored to the original scattering region. Here, the parallel and antiparallel configurations are defined by focusing on the same sublattices; the MTJ has the parallel (antiparallel) configurations when Ru/Cr-A sites of the left and right electrodes have the magnetic moments aligned parallelly (antiparallelly) [Fig. 1(b)].

For the calculation of the transmission, we use the PWCOND codes contained in the QE package [74–76]. Following the Landauer-Büttiker formula, the total conductance G is given by the total transmission T_{tot} as $G = (e^2/h)T_{tot}$ with the elementary charge e and the Planck constant h. The total transmission T_{tot} is calculated by summing up the transmission at each in-plane $\mathbf{k}_\parallel = (k_x, k_y)$ point perpendicular to the conducting path with spin-σ, $T_\sigma(\mathbf{k}_\parallel)$ as

$$T_{tot} = \sum_{\sigma=\uparrow,\downarrow} \frac{1}{N_{\mathbf{k}_\parallel}} \sum_{\mathbf{k}_\parallel} T_\sigma(\mathbf{k}_\parallel). \tag{1}$$

Here, the z direction, which is the conducting direction, is taken along the c axis of the MTJ [see also Fig. 1(b)], and $N_{\mathbf{k}_\parallel}$ is the number of $\mathbf{k}_\parallel$ point in the transmission calculation. We take $N_{\mathbf{k}_\parallel} = 251 \times 251$.
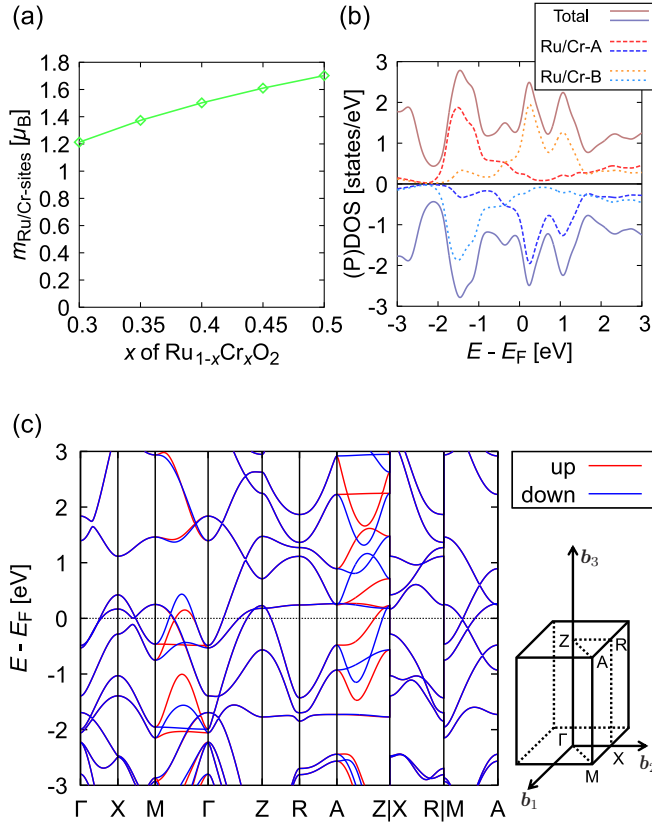
FIG. 2. (a) Averaged size of the magnetic moments of Ru(Cr) ions in $Ru_{1-x}Cr_xO_2$ with respect to the amount of Cr doping. (b) Spin-resolved density of states (DOS) and projected DOS (PDOS) of two Ru/Cr sites for $Ru_{0.65}Cr_{0.35}O_2$ as a function of energy. Positive (negative) values of the (P)DOS are the spin-up (down) components. (c) Energy band structure of $Ru_{0.65}Cr_{0.35}O_2$ resolved by the spin degrees of freedom. The high-symmetry points in the Brillouin zone for the tetragonal crystal structure are schematically shown on the right side of the energy band, where $\boldsymbol{b}_i$ ($i = 1, 2, 3$) is the primitive reciprocal lattice vector.

B. Evaluation of tunnel magnetoresistance effect with local density of states

Here, we briefly review the method which is used to qualitatively estimate the TMR effect with LDOS based on Ref. [33]. Using the conventional Jullire's picture, the transmission is approximated by the spin polarization, or equivalently, the total DOS, of the two magnetic metals used for the electrodes [1,2]. Specifically, τ_{DOS} is given as

$$\tau_{DOS} \sim \sum_{\sigma=\uparrow,\downarrow} D_{L,\sigma}(E) D_{R,\sigma}(E). \quad (2)$$

Here, $D_{L/R,\sigma}(E)$ is the density of states of the left/right electrodes.

In a similar manner to the Julliere's picture, we can consider the product of the LDOS inside the insulating barrier $d_{L/R,\sigma}(E)$,

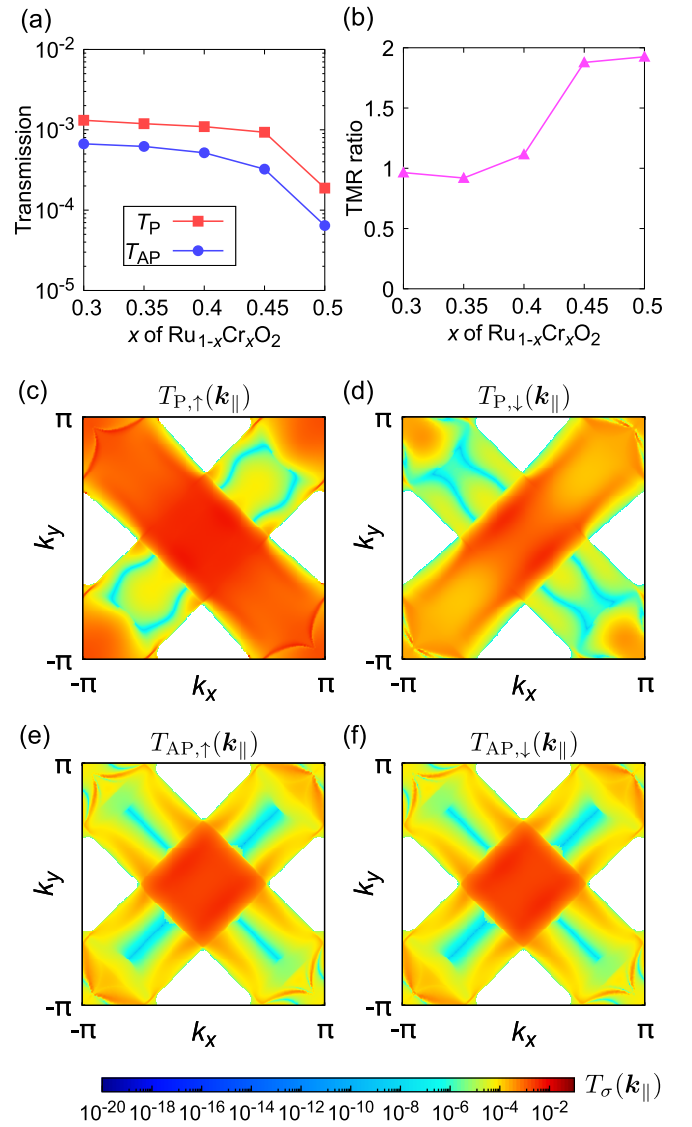$$\tau_{LDOS} \sim \sum_{i=1}^{n_a} \sum_{\sigma=\uparrow,\downarrow} d_{L,i,\sigma}(E) d_{R,i,\sigma}(E), \quad (3)$$

FIG. 3. (a) Cr-doping amount dependence of the total transmission for the parallel and antiparallel configurations of the $Ru_{1-x}Cr_xO_2/TiO_2/Ru_{1-x}Cr_xO_2$ magnetic tunnel junction. (b) TMR ratio calculated by $(T_P - T_{AP})/T_{AP}$. [(c)–(f)] Transmission resolved by the spin and the in-plane momentum $\boldsymbol{k}_\parallel$, $T_\sigma(\boldsymbol{k}_\parallel)$, for the $x = 0.35$ system. Transmission of (c) up and (d) down spins for the parallel configuration. Transmission of (e) up and (f) down spins for the antiparallel configuration.

where $d_{L/R,i,\sigma}(E)$ is the LDOS inside the barrier, and n_a is the number of atoms in the barrier layers which we focus on, layer-L and R. By using the LDOS inside the barrier instead of the DOS of the electrodes, we can take account of the details of the characters of materials used for the electrodes and barriers and also the decay inside the tunneling barrier, which is in sharp contrast to τ_{DOS} where only the bulk properties of the metals are considered.

To obtain the LDOS inside the barrier, we perform the non-scf calculation for the scattering region used in the transmission calculation, specifically, $Ru_{1-x}Cr_xO_2$ (4 MLs)/TiO_2 (9 MLs)/$Ru_{1-x}Cr_xO_2$ (5 MLs),
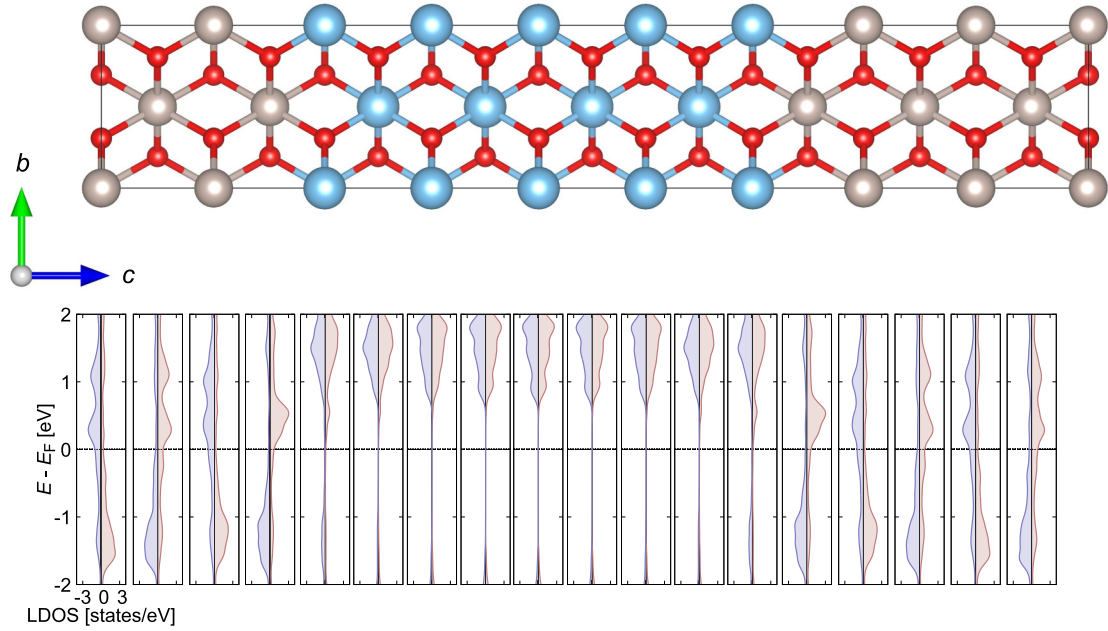
FIG. 4. Spin-resolved local density of states (LDOS) at each layer of the scattering region for the $x = 0.35$ system. Positive (negative) values of the LDOS represent the LDOS of the up (down) spin components.

or the aforementioned doubled supercell for the antiparallel configuration, with a $\mathbf{k}$-point mesh of $21 \times 21 \times 1$ following the scf calculation. Then, we calculate the projected DOS onto each atom. Here, we use the LDOS of the atoms in one layer away from the center of the barrier and take the product of the LDOS of the two atoms with the same xy coordinates [77].

III. RESULTS AND DISCUSSIONS

A. Bulk property of Cr-doped RuO$_2$

Before discussing the transmission properties of the MTJ with Cr-doped RuO$_2$, we discuss the bulk properties of Ru$_{1-x}$Cr$_x$O$_2$. We consider the systems with $0.3 \leqslant x \leqslant 0.5$ to ensure a large enough magnetic moment. In this region, the collinear antiferromagnetic state has a lower energy than the nonmagnetic state. We also confirm that the ferromag-
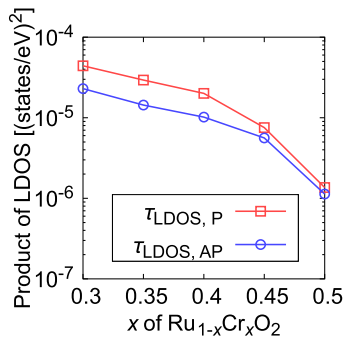

FIG. 5. Cr-concentration dependence of the product of the local density of states at the Fermi energy for parallel and antiparallel configurations calculated by Eq. (3).

netic state has a higher energy than the antiferromagnetic state for $0.3 \leqslant x \leqslant 0.5$ thereby excluding the possibility of realizing the ferromagnetic state as rutile-type CrO$_2$ exhibits a ferromagnetic state [78–81]. The comparison of the total energies of the nonmagnetic, ferromagnetic, and antiferromagnetic states is shown in Appendix. A.

In Fig. 2(a), we show the Cr concentration dependence of the magnitude of the magnetic moments in Ru$_{1-x}$Cr$_x$O$_2$. The size of the magnetic moments becomes larger as the amount of Cr doping increases, which is consistent with the results of the previous study showing that the magnetic moments of Ru ion increase by substituting the Ru ion with Cr ion [57]. This enhancement of the magnetic moment indicates that the Cr-doping strengthens the electronic correlation. It should be noted that the Coulomb U is not required to stabilize the magnetically ordered states here. To discuss RuO$_2$ as an antiferromagnet, calculations with additional U have been performed. However, in Ref. [54], it has been pointed out that the actual Ru materials have a relatively small U (U_{eff}) of $\lesssim 1$ eV, indicating that stoichiometric RuO$_2$ will not be an antiferromagnet. Also, the observed values of the magnetic moment of the Ru-ions are ~ 0.05 μ_{B} (0.23 μ_{B}) in the polarized (unpolarized) neutron diffraction measurement [49], which indicates that the electron correlation in RuO$_2$ is not likely to be large [82]. Therefore, we restrict ourselves to the case without $+U$. In our case, the realization of the magnetic state is attributed not to the effect of $+U$ but to the replacement of Ru-$4d$ electrons with Cr-$3d$ electrons. Hence, we expect to naturally describe the Ru-based materials here.

We show the total DOS and projected DOS (PDOS) of two Ru/Cr-sites resolved by the spin degrees of freedom for the $x = 0.35$ system in Fig. 2(b). The total DOS is symmetric with respect to the spin degrees of freedom, which suggests that the magnetization in Ru$_{1-x}$Cr$_x$O$_2$ is compensated overall. We
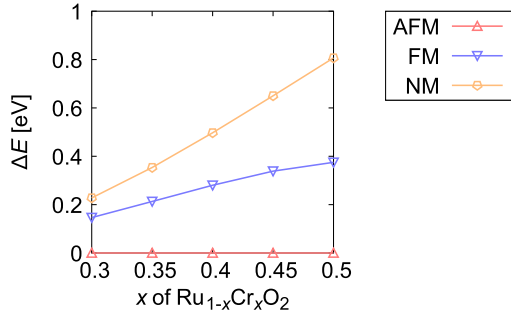
FIG. 6. Cr-concentration dependence of the total energies of the antiferromagnetic (AFM), ferromagnetic (FM), and nonmagnetic (NM) states. The energy differences with the energy of the AFM states are shown.

also find that each of the two Ru/Cr-sites in a unit cell has the spin-polarized PDOS, consistent with the presence of finite magnetic moments of Ru sites.

Figure 2(c) shows the energy band structure of $Ru_{1-x}Cr_xO_2$. We see the spin splitting along $M-\Gamma$ and $A-Z$ lines in the momentum space, where $|k_x| = |k_y|$. which is the same as the spin splitting band observed in the pure RuO_2 [44,46].

B. Tunnel magnetoresistance effect with Cr-doped RuO_2 electrode

Next, we discuss the TMR effect in the $Ru_{1-x}Cr_xO_2/TiO_2/Ru_{1-x}Cr_xO_2$ MTJ. In Fig. 3(a), we show the Cr concentration dependence of the total transmission T_{tot} of the parallel and antiparallel configurations at the Fermi level, T_P and T_{AP}, respectively. Both T_P and T_{AP} decrease as the amount of the Cr-doping increases. In $0.3 \leqslant x \leqslant 0.5$, T_P is larger than T_{AP}. This means that the corresponding TMR ratio, defined by $(T_P - T_{AP})/T_{AP}$, takes positive finite values as shown in Fig. 3(b). The TMR ratio is around 100%–200%. This value is smaller than that in the $RuO_2/TiO_2/RuO_2$ MTJ [29]. Still, we should note that a large U is often assumed for RuO_2, which possibly overestimate the magnetism of pure RuO_2 as discussed in Sec. III A. In addition, we do not add the Coulomb U here, which makes us underestimate the energy gap of TiO_2 here. If we take the effect of $+U$ into account and evaluate the band gap of TiO_2 more accurately, the TMR ratio in the $Ru_{1-x}Cr_xO_2$-based MTJ may become as large as that in the RuO_2-based MTJ, which we leave as the future work.

In Figs. 3(c)–3(f), we show the transmission at the Fermi level resolved by the in-plane momentum perpendicular to the conducting path $\boldsymbol{k}_\parallel$ for the $x = 0.35$ system. For the parallel configuration, the transmission takes a large value near the $|k_x| = |k_y|$ line, where the spin splitting of $Ru_{1-x}Cr_xO_2$ is present as seen in the band structure shown in Fig. 2(b). For the antiparallel configuration, since the two magnetic electrodes have the opposite spin polarization with each other, $T(\boldsymbol{k}_\parallel)$ around the Γ point takes a large value.

It should be stressed that the transport discussed here is the tunneling one. We show the energy dependence of the LDOS of each layer of the scattering region for the parallel configuration with $x = 0.35$ in Fig. 4. We find that the LDOS
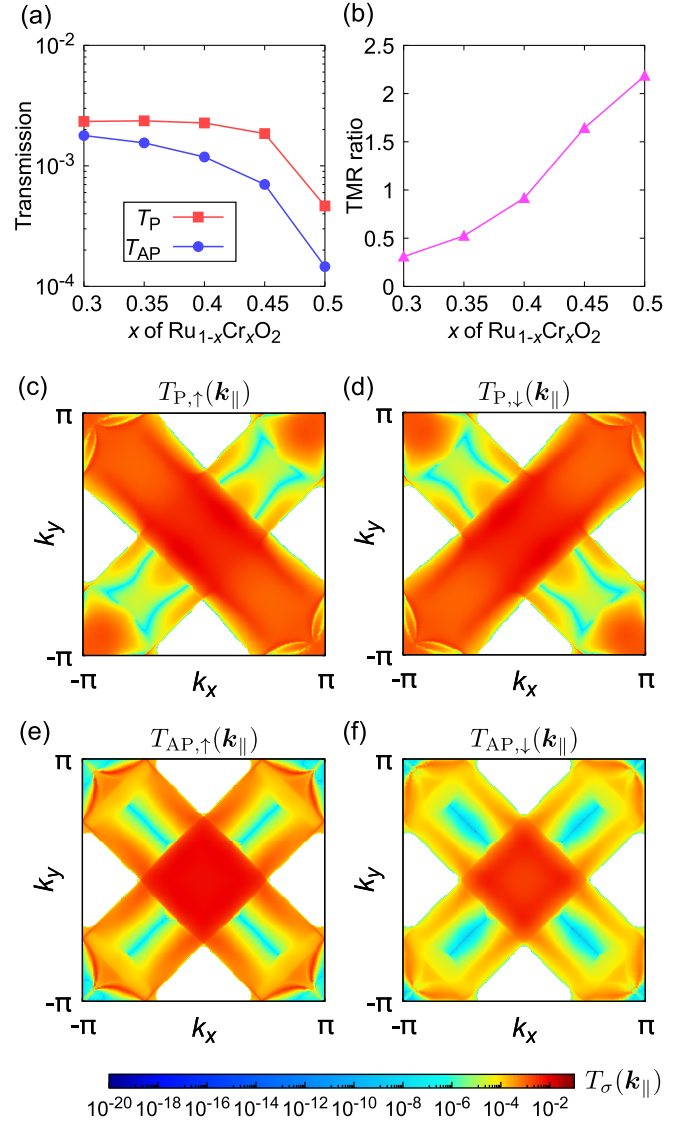

FIG. 7. Results of the transmission calculation with eight monolayers of TiO_2. (a) Total transmission with respect to the amount of Cr doping. (b) TMR ratio. (c)–(f) Momentum resolved transmission for the $x = 0.35$ system. (c) Up and (d) down spins for the parallel configuration. (e) Up and (f) down spins for the antiparallel configuration.

in the TiO_2 layers is small enough around the Fermi level. Namely, the Fermi level of the scattering region is well inside the band gap of TiO_2, which ensures the tunneling transport.

We also calculate the TMR effect for the MTJ with eight MLs of TiO_2 to check the effect of the magnetic moments at the interface. In the MTJ with nine MLs or odd numbers of MLs of TiO_2, the interfacial magnetic moments of the two magnetic electrodes align parallelly (antiparallelly) for the parallel (antiparallel) configuration, as schematically shown in Fig. 1(b). When the number of layers is even, the magnetic moments at the interface of the electrodes align antiparallel for the parallel configuration of the MTJ, and parallel for the antiparallel configuration. This difference of the relative directions of the interfacial magnetic moments may influence the TMR effect. However, for the present case, we obtain

similar TMR properties in the range $0.3 \leqslant x \leqslant 0.5$ between the MTJ with nine MLs of TiO_2 and the one with eight MLs of TiO_2, indicating that the interfacial magnetic structure does not qualitatively affect the TMR properties in this region. See Appendix B for detailed results.

In our previous calculations using the lattice model, we have pointed out that the TMR ratio can change its sign depending on the relative alignments of the interfacial magnetic moments of the two electrodes when using the magnets with multiple sublattices, such as the ferrimagnets or antiferromagnets [33]. However, the situation is different between that lattice model and the current system, the $Ru_{1-x}Cr_xO_2/TiO_2/Ru_{1-x}Cr_xO_2$-MTJ. In the model calculation, we have considered the relative alignments of two magnetic moments at the interface, which had the same in-plane coordinates perpendicular to the conducting path. In contrast, in the present case, the interfacial magnetic moments of the two electrodes have different in-plane positions. The magnetic moments of the two electrodes with the same in-plane positions align parallelly (antiparallelly) for the parallel (antiparallel) configuration regardless of the number of barrier layers.

C. Local density of states inside the barrier

Finally, we discuss the correspondence between the transmission and the LDOS inside the barrier. Recent studies have revealed that the LDOS inside the barrier can evaluate the TMR effect more precisely [18,33]. While the $\boldsymbol{k}$-space picture of the LDOS [18] can also be adopted, here we use the real-space approach [33]. Figure 5 shows the product of the LDOS at the Fermi energy calculated following Eq. (3) with respect to the amount of Cr. We find that the product of the LDOS decreases for each of the parallel and antiparallel configurations, and $\tau_{\text{LDOS, P}}$ takes larger values than $\tau_{\text{LDOS, AP}}$. These features are consistent with the transmission property shown in Fig. 3(b), indicating that we can qualitatively capture the transmission behavior using the LDOS not only in the idealized lattice models [33] but also in a realistic system.

IV. SUMMARY

In summary, we have discussed the tunnel magnetoresistance (TMR) effect using the Cr-doped RuO_2 as an electrode of the magnetic tunnel junction (MTJ) from first-principles calculations. We have performed *ab initio* calculation of the tunneling conductance in the $Ru_{1-x}Cr_xO_2/TiO_2/Ru_{1-x}Cr_xO_2$ MTJ. We have found that a finite TMR effect is generated by a finite spin splitting in the momentum space, which is

supported by the enhancement of the electron correlation in $Ru_{1-x}Cr_xO_2$ owing to the Cr doping. We have also shown that the qualitative nature of the obtained TMR effect can be traced using the local density of states (LDOS) inside the barrier of the MTJ. We believe that this correspondence between the TMR property and the LDOS in realistic systems will be helpful in searching for materials suitable for MTJs.

APPENDIX A: COMPARISON OF TOTAL ENERGY OF DIFFERENT MAGNETIC STATES

In Fig. 6, we plot the total energies of the nonmagnetic, ferromagnetic, and antiferromagnetic states of $Ru_{1-x}Cr_xO_2$ with respect to the amount of Cr. This result shows that the antiferromagnetic state takes lower energy than the other two states.

APPENDIX B: TRANSMISSION WITH EVEN NUMBER OF BARRIER LAYERS: EFFECT OF INTERFACIAL MAGNETIC MOMENTS

In the main text, we have discussed the TMR effect in the MTJ with nine MLs of TiO_2. To check the effect of the magnetic moments at the interface, we calculate the TMR effect with eight MLs of TiO_2. For the scattering region, we use the eight MLs of TiO_2 with four MLs of $Ru_{1-x}Cr_xO_2$ attached to both sides.

We present the results of the transmission calculation in Fig. 7. As shown in Figs. 7(a) and 7(b), T_P takes a larger value than T_{AP} in $0.3 \leqslant x \leqslant 0.5$, and thus the TMR ratio is positive, which is qualitatively the same as the case with nine MLs of TiO_2. Also, the momentum resolved transmissions for the $x = 0.35$ system shown in Figs. 7(c)–7(f) exhibit similar structures to those in the MTJ with nine MLs of TiO_2 [see Figs. 3(c)–3(f)]. Hence, the magnetic moments at the interface do not change the TMR properties qualitatively in this region.

[1] M. Julliere, Tunneling between ferromagnetic films, Phys. Lett. A **54**, 225 (1975).

[2] S. Maekawa and U. Gafvert, Electron tunneling between ferromagnetic films, IEEE Trans. Magn. **18**, 707 (1982).

[3] J. C. Slonczewski, Conductance and exchange coupling of two ferromagnets separated by a tunneling barrier, Phys. Rev. B **39**, 6995 (1989).

[4] T. Miyazaki and N. Tezuka, Giant magnetic tunneling effect in Fe/Al$_2$O$_3$/Fe junction, J. Magn. Magn. Mater. **139**, L231 (1995).

[5] J. S. Moodera, L. R. Kinder, T. M. Wong, and R. Meservey, Large magnetoresistance at room temperature in ferromagnetic thin film tunnel junctions, Phys. Rev. Lett. **74**, 3273 (1995).

[6] J. Mathon, Tight-binding theory of tunneling giant magnetoresistance, Phys. Rev. B **56**, 11810 (1997).

[7] W. H. Butler, X.-G. Zhang, T. C. Schulthess, and J. M. MacLaren, Spin-dependent tunneling conductance of Fe|MgO|Fe sandwiches, Phys. Rev. B **63**, 054416 (2001).

[8] J. Mathon and A. Umerski, Theory of tunneling magnetoresistance of an epitaxial Fe/MgO/Fe(001) junction, Phys. Rev. B **63**, 220403(R) (2001).

[9] S. S. Parkin, C. Kaiser, A. Panchula, P. M. Rice, B. Hughes, M. Samant, and S.-H. Yang, Giant tunnelling magnetoresistance at room temperature with MgO (100) tunnel barriers, Nat. Mater. **3**, 862 (2004).

[10] K. D. Belashchenko, E. Y. Tsymbal, M. van Schilfgaarde, D. A. Stewart, I. I. Oleynik, and S. S. Jaswal, Effect of interface bonding on spin-dependent tunneling from the oxidized Co surface, Phys. Rev. B **69**, 174408 (2004).

[11] S. Yuasa, T. Nagahama, A. Fukushima, Y. Suzuki, and K. Ando, Giant room-temperature magnetoresistance in single-crystal Fe/MgO/Fe magnetic tunnel junctions, Nat. Mater. **3**, 868 (2004).

[12] E. Y. Tsymbal and K. D. Belashchenko, Role of interface bonding in spin-dependent tunneling (invited), J. Appl. Phys. **97**, 10C910 (2005).

[13] E. Y. Tsymbal, K. D. Belashchenko, J. P. Velev, S. S. Jaswal, M. van Schilfgaarde, I. I. Oleynik, and D. A. Stewart, Interface effects in spin-dependent tunneling, Prog. Mater. Sci. **52**, 401 (2007).

[14] S. Ikeda, J. Hayakawa, Y. Ashizawa, Y. M. Lee, K. Miura, H. Hasegawa, M. Tsunoda, F. Matsukura, and H. Ohno, Tunnel magnetoresistance of 604% at 300 K by suppression of Ta diffusion in CoFeB/MgO/CoFeB pseudo-spin-valves annealed at high temperature, Appl. Phys. Lett. **93**, 082508 (2008).

[15] S. Ikeda, K. Miura, H. Yamamoto, K. Mizunuma, H. Gan, M. Endo, S. Kanai, J. Hayakawa, F. Matsukura, and H. Ohno, A perpendicular-anisotropy CoFeB–MgO magnetic tunnel junction, Nat. Mater. **9**, 721 (2010).

[16] D. C. Worledge, G. Hu, D. W. Abraham, J. Z. Sun, P. L. Trouilloud, J. Nowak, S. Brown, M. C. Gaidis, E. J. O'Sullivan, and R. P. Robertazzi, Spin torque switching of perpendicular Ta | CoFeB | MgO-based magnetic tunnel junctions, Appl. Phys. Lett. **98**, 022501 (2011).

[17] T. Scheike, Z. Wen, H. Sukegawa, and S. Mitani, 631% room temperature tunnel magnetoresistance with large oscillation effect in CoFe/MgO/CoFe(001) junctions, Appl. Phys. Lett. **122**, 112404 (2023).

[18] G. G. B. Flores, M. van Schilfgaarde, and K. D. Belashchenko, Tunneling magnetoresistance in MgO tunnel junctions with Fe-based leads in empirically corrected density functional theory, arXiv:2404.08103.

[19] E. Y. Tsymbal, O. N. Mryasov, and P. R. LeClair, Spin-dependent tunnelling in magnetic tunnel junctions, J. Phys.: Condens. Matter **15**, R109 (2003).

[20] X.-G. Zhang and W. H. Butler, Band structure, evanescent states, and transport in spin tunnel junctions, J. Phys.: Condens. Matter **15**, R1603 (2003).

[21] H. Itoh and J. Inoue, Theory of tunnel magnetoresistance, J. Magn. Soc. Jpn. **30**, 1 (2006).

[22] S. Yuasa and D. D. Djayaprawira, Giant tunnel magnetoresistance in magnetic tunnel junctions with a crystalline MgO(001) barrier, J. Phys. D: Appl. Phys. **40**, R337 (2007).

[23] W. H. Butler, Tunneling magnetoresistance from a symmetry filtering effect, Sci. Technol. Adv. Mater. **9**, 014106 (2008).

[24] X. Chen, T. Higo, K. Tanaka, T. Nomoto, H. Tsai, H. Idzuchi, M. Shiga, S. Sakamoto, R. Ando, H. Kosaki *et al.*, Octupole-driven magnetoresistance in an antiferromagnetic tunnel junction, Nature (London) **613**, 490 (2023).

[25] P. Merodio, A. Kalitsov, H. Béa, V. Baltz, and M. Chshiev, Spin-dependent transport in antiferromagnetic tunnel junctions, Appl. Phys. Lett. **105**, 122403 (2014).

[26] M. Stamenova, R. Mohebbi, J. Seyed-Yazdi, I. Rungger, and S. Sanvito, First-principles spin-transfer torque in CuMnAs|GaP|CuMnAs junctions, Phys. Rev. B **95**, 060403(R) (2017).

[27] J. Železný, Y. Zhang, C. Felser, and B. Yan, Spin-polarized current in noncollinear antiferromagnets, Phys. Rev. Lett. **119**, 187204 (2017).

[28] X.-T. Jia, X.-L. Cai, and Y. Jia, Giant magnetoresistance in antiferromagnetic Mn_2Au-based tunnel junction, Sci. China Math. **63**, 297512 (2020).

[29] D.-F. Shao, S.-H. Zhang, M. Li, C.-B. Eom, and E. Y. Tsymbal, Spin-neutral currents for spintronics, Nat. Commun. **12**, 7061 (2021).

[30] L. Šmejkal, A. B. Hellenes, R. González-Hernández, J. Sinova, and T. Jungwirth, Giant and tunneling magnetoresistance in unconventional collinear antiferromagnets with nonrelativistic spin-momentum coupling, Phys. Rev. X **12**, 011028 (2022).

[31] J. Dong, X. Li, G. Gurung, M. Zhu, P. Zhang, F. Zheng, E. Y. Tsymbal, and J. Zhang, Tunneling magnetoresistance in noncollinear antiferromagnetic tunnel junctions, Phys. Rev. Lett. **128**, 197201 (2022).

[32] P. Qin, H. Yan, X. Wang, H. Chen, Z. Meng, J. Dong, M. Zhu, J. Cai, Z. Feng, X. Zhou *et al.*, Room-temperature magnetoresistance in an all-antiferromagnetic tunnel junction, Nature (London) **613**, 485 (2023).

[33] K. Tanaka, T. Nomoto, and R. Arita, Local density of states as a probe for tunneling magnetoresistance effect: Application to ferrimagnetic tunnel junctions, Phys. Rev. B **107**, 214442 (2023).

[34] Q. Cui, Y. Zhu, X. Yao, P. Cui, and H. Yang, Giant spin-Hall and tunneling magnetoresistance effects based on a two-dimensional nonrelativistic antiferromagnetic metal, Phys. Rev. B **108**, 024410 (2023).

[35] G. Gurung, D.-F. Shao, and E. Y. Tsymbal, Extraordinary tunneling magnetoresistance in antiferromagnetic tunnel junctions with antiperovskite electrodes, arXiv:2306.03026.

[36] X. Jia, H.-M. Tang, and S.-Z. Wang, Tunneling magnetoresistance in all-antiferromagnetic Mn_2 Au-based tunnel junctions, Phys. Rev. B **108**, 104406 (2023).

[37] Y.-Y. Jiang, Z.-A. Wang, K. Samanta, S.-H. Zhang, R.-C. Xiao, W. J. Lu, Y. P. Sun, E. Y. Tsymbal, and D.-F. Shao, Prediction of giant tunneling magnetoresistance in $RuO_2/TiO_2/RuO_2$ (110) antiferromagnetic tunnel junctions, Phys. Rev. B **108**, 174439 (2023).

[38] B. Chi, L. Jiang, Y. Zhu, G. Yu, C. Wan, J. Zhang, and X. Han, Crystal-facet-oriented altermagnets for detecting ferromagnetic and antiferromagnetic states by giant tunneling magnetoresistance, Phys. Rev. Applied **21**, 034038 (2024).

[39] K. Samanta, Y.-Y. Jiang, T. R. Paudel, D.-F. Shao, and E. Y. Tsymbal, Tunneling magnetoresistance in magnetic tunnel

junctions with a single ferromagnetic electrode, Phys. Rev. B **109**, 174407 (2024).

[40] J. Shi, S. Arpaci, V. Lopez-Dominguez, V. K. Sangwan, F. Mahfouzi, J. Kim, J. G. Athas, M. Hamdi, C. Aygen, H. Arava, C. Phatak, M. Carpentieri, J. S. Jiang, M. A. Grayson, N. Kioussis, G. Finocchio, M. C. Hersam, and P. K. Amiri, Electrically controlled all-antiferromagnetic tunnel junctions on silicon with large room-temperature magnetoresistance, Adv. Mater. **36**, 2312008 (2024).

[41] C. Zhu, X. Jia, and H.-M. Tang, Tunneling magnetoresistance effect in antiferromagnetic $Mn_2Au/BAs/Mn_2Au$ tunnel junctions, J. Magn. Magn. Mater. **597**, 172036 (2024).

[42] D.-F. Shao and E. Y. Tsymbal, Antiferromagnetic tunnel junctions for spintronics, npj Spintronics **2**, 13 (2024).

[43] Y. Noda, K. Ohno, and S. Nakamura, Momentum-dependent band spin splitting in semiconducting MnO_2: A density functional calculation, Phys. Chem. Chem. Phys. **18**, 13294 (2016).

[44] K.-H. Ahn, A. Hariki, K.-W. Lee, and J. Kuneš, Antiferromagnetism in RuO_2 as d-wave Pomeranchuk instability, Phys. Rev. B **99**, 184432 (2019).

[45] M. Naka, S. Hayami, H. Kusunose, Y. Yanagi, Y. Motome, and H. Seo, Spin current generation in organic antiferromagnets, Nat. Commun. **10**, 4305 (2019).

[46] L. Šmejkal, R. González-Hernández, T. Jungwirth, and J. Sinova, Crystal time-reversal symmetry breaking and spontaneous Hall effect in collinear antiferromagnets, Sci. Adv. **6**, eaaz8809 (2020).

[47] L. Šmejkal, J. Sinova, and T. Jungwirth, Beyond conventional ferromagnetism and antiferromagnetism: A phase with nonrelativistic spin and crystal rotation symmetry, Phys. Rev. X **12**, 031042 (2022).

[48] L. Šmejkal, J. Sinova, and T. Jungwirth, Emerging research landscape of altermagnetism, Phys. Rev. X **12**, 040501 (2022).

[49] T. Berlijn, P. C. Snijders, O. Delaire, H.-D. Zhou, T. A. Maier, H.-B. Cao, S.-X. Chi, M. Matsuda, Y. Wang, M. R. Koehler, P. R. C. Kent, and H. H. Weitering, Itinerant antiferromagnetism in RuO_2, Phys. Rev. Lett. **118**, 077201 (2017).

[50] Z. H. Zhu, J. Strempfer, R. R. Rao, C. A. Occhialini, J. Pelliciari, Y. Choi, T. Kawaguchi, H. You, J. F. Mitchell, Y. Shao-Horn, and R. Comin, Anomalous antiferromagnetism in metallic RuO_2 determined by resonant x-ray scattering, Phys. Rev. Lett. **122**, 017202 (2019).

[51] O. Fedchenko, J. Minár, A. Akashdeep, S. W. D'Souza, D. Vasilyev, O. Tkach, L. Odenbreit, Q. Nguyen, D. Kutnyakhov, N. Wind *et al.*, Observation of time-reversal symmetry breaking in the band structure of altermagnetic RuO_2, Sci. Adv. **10**, eadj4883 (2024).

[52] Z. Feng, X. Zhou, L. Šmejkal, L. Wu, Z. Zhu, H. Guo, R. González-Hernández, X. Wang, H. Yan, P. Qin *et al.*, An anomalous Hall effect in altermagnetic ruthenium dioxide, Nat. Electron. **5**, 735 (2022).

[53] D.-F. Shao, Y.-Y. Jiang, J. Ding, S.-H. Zhang, Z.-A. Wang, R.-C. Xiao, G. Gurung, W. J. Lu, Y. P. Sun, and E. Y. Tsymbal, Néel spin currents in antiferromagnets, Phys. Rev. Lett. **130**, 216702 (2023).

[54] A. Smolyanyuk, I. I. Mazin, L. Garcia-Gassull, and R. Valentí, Fragility of the magnetic order in the prototypical altermagnet RuO_2, Phys. Rev. B **109**, 134424 (2024).

[55] M. Hiraishi, H. Okabe, A. Koda, R. Kadono, T. Muroi, D. Hirai, and Z. Hiroi, Nonmagnetic ground state in RuO_2 revealed by muon spin rotation, Phys. Rev. Lett. **132**, 166702 (2024).

[56] P. Keßler, L. Garcia-Gassull, A. Suter, T. Prokscha, Z. Salman, D. Khalyavin, P. Manuel, F. Orlandi, I. I. Mazin, R. Valentí, and S. Moser, Absence of magnetic order in RuO_2: Insights from μSR spectroscopy and neutron diffraction, arXiv:2405.10820.

[57] M. Wang, K. Tanaka, S. Sakai, Z. Wang, K. Deng, Y. Lyu, C. Li, D. Tian, S. Shen, N. Ogawa *et al.*, Emergent zero-field anomalous Hall effect in a reconstructed rutile antiferromagnetic metal, Nat. Commun. **14**, 8240 (2023).

[58] D. Zagorac, H. Müller, S. Ruehl, J. Zagorac, and S. Rehme, Recent developments in the Inorganic Crystal Structure Database: Theoretical crystal structure data and related features, J. Appl. Crystallogr. **52**, 918 (2019).

[59] H. J. Choi and J. Ihm, *Ab initio* pseudopotential method for the calculation of conductance in quantum wires, Phys. Rev. B **59**, 2267 (1999).

[60] R. Landauer, Spatial variation of currents and fields due to localized scatterers in metallic conduction, IBM J. Res. Dev. **1**, 223 (1957).

[61] R. Landauer, Electrical resistance of disordered one-dimensional lattices, Philos. Mag. **21**, 863 (1970).

[62] M. Büttiker, Four-terminal phase-coherent conductance, Phys. Rev. Lett. **57**, 1761 (1986).

[63] M. Büttiker, Symmetry of electrical conduction, IBM J. Res. Dev. **32**, 317 (1988).

[64] P. Hohenberg and W. Kohn, Inhomogeneous electron gas, Phys. Rev. **136**, B864 (1964).

[65] W. Kohn and L. J. Sham, Self-consistent equations including exchange and correlation effects, Phys. Rev. **140**, A1133 (1965).

[66] P. Giannozzi, S. Baroni, N. Bonini, M. Calandra, R. Car, C. Cavazzoni, D. Ceresoli, G. L. Chiarotti, M. Cococcioni, I. Dabo *et al.*, QUANTUM ESPRESSO: A modular and open-source software project for quantum simulations of materials, J. Phys.: Condens. Matter **21**, 395502 (2009).

[67] P. Giannozzi, O. Andreussi, T. Brumme, O. Bunau, M. B. Nardelli, M. Calandra, R. Car, C. Cavazzoni, D. Ceresoli, M. Cococcioni *et al.*, Advanced capabilities for materials modelling with QUANTUM ESPRESSO, J. Phys.: Condens. Matter **29**, 465901 (2017).

[68] D. R. Hamann, Optimized norm-conserving Vanderbilt pseudopotentials, Phys. Rev. B **88**, 085117 (2013).

[69] M. van Setten, M. Giantomassi, E. Bousquet, M. Verstraete, D. Hamann, X. Gonze, and G.-M. Rignanese, The PSEUDODOJO: Training and grading a 85 element optimized norm-conserving pseudopotential table, Comput. Phys. Commun. **226**, 39 (2018).

[70] J. P. Perdew, K. Burke, and M. Ernzerhof, Generalized gradient approximation made simple, Phys. Rev. Lett. **77**, 3865 (1996).

[71] L. Nordheim, Zur Elektronentheorie der Metalle. I, Ann. Phys. (NY) **401**, 607 (1931).

[72] L. Bellaiche and D. Vanderbilt, Virtual crystal approximation revisited: Application to dielectric and piezoelectric properties of perovskites, Phys. Rev. B **61**, 7877 (2000).

[73] The VCA calculation in this paper overestimates the size of the magnetic moments of Cr-doped RuO_2, which we confirm the

supercell calculation with 50% doping of Cr. When we compare the systems with similar sizes of the (averaged) magnetic moments, e.g., the VCA system with $x = 0.3$ and the supercell with 50% doping, we can observe the spin splitting on the same energy scale.

[74] A. Smogunov, A. Dal Corso, and E. Tosatti, Ballistic conductance of magnetic Co and Ni nanowires with ultrasoft pseudopotentials, Phys. Rev. B **70**, 045417 (2004).

[75] A. Dal Corso and A. Mosca Conte, Spin-orbit coupling with ultrasoft pseudopotentials: Application to Au and Pt, Phys. Rev. B **71**, 115106 (2005).

[76] A. Dal Corso, A. Smogunov, and E. Tosatti, *Ab initio* ballistic conductance with spin-orbit coupling: Application to monoatomic wires, Phys. Rev. B **74**, 045429 (2006).

[77] For the antiparallel configuration, we use the LDOS of the first half of the doubled scattering region.

[78] B. L. Chamberland, The chemical and physical properties of CrO_2 and tetravalent chromium oxide derivatives, Crit. Rev. Solid State Mater. Sci. **7**, 1 (1977).

[79] K. Schwarz, CrO_2 predicted as a half-metallic ferromagnet, J. Phys. F: Met. Phys. **16**, L211 (1986).

[80] M. A. Korotin, V. I. Anisimov, D. I. Khomskii, and G. A. Sawatzky, CrO_2: A self-doped double exchange ferromagnet, Phys. Rev. Lett. **80**, 4305 (1998).

[81] J. H. Shim, S. Lee, J. Dho, and D.-H. Kim, Coexistence of two different Cr ions by self-doping in half-metallic CrO_2 nanorods, Phys. Rev. Lett. **99**, 057209 (2007).

[82] We evaluate the Coulomb U of the Ru atoms in RuO_2 using the density functional perturbation theory (DFPT) calculation [85]. The obtained values of U are $\gtrsim 4-5$ eV, though the detailed values change depending on the choice of initial conditions, such as the pseudopotential or the projection type in the DFT $+ U$ calculation.

[83] K. Momma and F. Izumi, *VESTA3* for three-dimensional visualization of crystal, volumetric and morphology data, J. Appl. Crystallogr. **44**, 1272 (2011).

[84] A. Kokalj, XCrySDen—A new program for displaying crystalline structures and electron densities, J. Mol. Graphics Modell. **17**, 176 (1999).

[85] I. Timrov, N. Marzari, and M. Cococcioni, Hubbard parameters from density-functional perturbation theory, Phys. Rev. B **98**, 085127 (2018).